High efficiency fabrication of complex microtube arrays by scanning focused femtosecond laser Bessel beam for trapping/releasing biological cells

LIANG YANG,[1] SHENGYUN JI,[1] KENAN XIE,[2] WENQIANG DU,[1] BINGJIE LIU,[3] YANLEI HU,[1] JIAWEN LI,[1,4] GANG ZHAO,[1] DONG WU,[1,*] WENHAO HUANG,[1] SULING LIU,[3] HONGYUAN JIANG,[2] AND JIARU CHU[1]

[1]*CAS Key Laboratory of Mechanical Behavior and Design of Materials, Department of Precision Machinery and Precision Instrumentation, University of Science and Technology of China, Hefei 230026, China*
[2]*Department of Modern Mechanics, University of Science and Technology of China, Hefei 230026, China*
[3]*School of Life Sciences, University of Science and Technology of China, Hefei 230026, China*
[4]*jwl@ustc.edu.cn*
*dongwu@ustc.edu.cn

Abstract: In this paper, we present a focused femtosecond laser Bessel beam scanning technique for the rapid fabrication of large-area 3D complex microtube arrays. The femtosecond laser beam is converted into several Bessel beams by two-dimensional phase modulation using a spatial light modulator. By scanning the focused Bessel beam along a designed route, microtubes with variable size and flexible geometry are rapidly fabricated by two-photon polymerization. The fabrication time is reduced by two orders of magnitude in comparison with conventional point-to-point scanning. Moreover, we construct an effective microoperating system for single cell manipulation using microtube arrays, and demonstrate its use in the capture, transfer, and release of embryonic fibroblast mouse cells as well as human breast cancer cells. The new fabrication strategy provides a novel method for the rapid fabrication of functional devices using a flexibly tailored laser beam.

References and links

1. W. Yan, M. M. Hossain, and M. Gu, "High light-directing micrometer-sized parabolic mirror arrays," Opt. Lett. **38**(16), 3177–3180 (2013).
2. J. A. Fu, H. T. Dong, and W. Fang, "Subwavelength focusing of light by a tapered microtube," Appl. Phys. Lett. **97**(4), 041114 (2010).
3. T. Kipp, H. Welsch, Ch. Strelow, Ch. Heyn, and D. Heitmann, "Optical modes in semiconductor microtube ring resonators," Phys. Rev. Lett. **96**(7), 077403 (2006).
4. S. D. Gittard, R. J. Narayan, C. Jin, A. Ovsianikov, B. N. Chichkov, N. A. Monteiro-Riviere, S. Stafslien, and B. Chisholm, "Pulsed laser deposition of antimicrobial silver coating on Ormocer microneedles," Biofabrication **1**(4), 041001 (2009).
5. K. Takei, T. Kawashima, T. Kawano, H. Kaneko, K. Sawada, and M. Ishida, "Out-of-plane microtube arrays for drug delivery--liquid flow properties and an application to the nerve block test," Biomed. Microdevices **11**(3), 539–545 (2009).
6. Z. Xiang, H. Wang, A. Pant, G. Pastorin, and C. Lee, "Development of vertical SU-8 microtubes integrated with dissolvable tips for transdermal drug delivery," Biomicrofluidics **7**(2), 026502 (2013).
7. S. D. Gittard, A. Nguyen, K. Obata, A. Koroleva, R. J. Narayan, and B. N. Chichkov, "Fabrication of microscale medical devices by two-photon polymerization with multiple foci via a spatial light modulator," Biomed. Opt. Express **2**(11), 3167–3178 (2011).
8. D. J. Thurmer, C. Deneke, Y. F. Mei, and O. G. Schmidt, "Process integration of microtubes for fluidic applications," Appl. Phys. Lett. **89**(22), 223507 (2006).

9. Y. Mei, A. A. Solovev, S. Sanchez, and O. G. Schmidt, "Rolled-up nanotech on polymers: from basic perception to self-propelled catalytic microengines," Chem. Soc. Rev. **40**(5), 2109–2119 (2011).
10. F. Mou, Y. Li, C. Chen, W. Li, Y. Yin, H. Ma, and J. Guan, "Single-component TiO$_2$ tubular microengines with motion controlled by light-induced bubbles," Small **11**(21), 2564–2570 (2015).
11. A. Martín, B. Jurado-Sánchez, A. Escarpa, and J. Wang, "Template electrosynthesis of high-performance graphene microengines," Small **11**(29), 3568–3574 (2015).
12. E. J. Smith, S. Schulze, S. Kiravittaya, Y. Mei, S. Sanchez, and O. G. Schmidt, "Lab-in-a-tube: detection of individual mouse cells for analysis in flexible split-wall microtube resonator sensors," Nano Lett. **11**(10), 4037–4042 (2011).
13. S. Sánchez, "Lab-in-a-tube systems as ultra-compact devices," Lab Chip **15**(3), 610–613 (2015).
14. C. S. Martinez-Cisneros, S. Sanchez, W. Xi, and O. G. Schmidt, "Ultracompact three-dimensional tubular conductivity microsensors for ionic and biosensing applications," Nano Lett. **14**(4), 2219–2224 (2014).
15. W. Xi, C. K. Schmidt, S. Sanchez, D. H. Gracias, R. E. Carazo-Salas, S. P. Jackson, and O. G. Schmidt, "Rolled-up functionalized nanomembranes as three-dimensional cavities for single cell studies," Nano Lett. **14**(8), 4197–4204 (2014).
16. G. Huang, Y. Mei, D. J. Thurmer, E. Coric, and O. G. Schmidt, "Rolled-up transparent microtubes as two-dimensionally confined culture scaffolds of individual yeast cells," Lab Chip **9**(2), 263–268 (2009).
17. S. Zakharchenko, E. Sperling, and L. Ionov, "Fully biodegradable self-rolled polymer tubes: a candidate for tissue engineering scaffolds," Biomacromolecules **12**(6), 2211–2215 (2011).
18. A. A. Solovev, W. Xi, D. H. Gracias, S. M. Harazim, C. Deneke, S. Sanchez, and O. G. Schmidt, "Self-propelled nanotools," ACS Nano **6**(2), 1751–1756 (2012).
19. K. H. Won, B. M. Weon, and J. H. Je, "Polymer composite microtube array produced by meniscus-guided approach," AIP Adv. **3**(9), 092127 (2013).
20. A. Sitt, J. Soukupova, D. Miller, D. Verdi, R. Zboril, H. Hess, and J. Lahann, "Microscale rockets and picoliter containers engineered from electrospun polymeric microtubes," Small **12**(11), 1432–1439 (2016).
21. X. H. Tan, T. L. Shi, Y. Gao, W. J. Sheng, B. Sun, and G. L. Liao, "Fabrication of micro/nanotubes by mask-based diffraction lithography," J. Micromech. Microeng. **24**(5), 055006 (2014).
22. W. Gao and J. Wang, "The environmental impact of micro/nanomachines: a review," ACS Nano **8**(4), 3170–3180 (2014).
23. E. Stankevicius, T. Gertus, M. Rutkauskas, M. Gedvilas, G. Raciukaitis, R. Gadonas, V. Smilgevicius, and M. Malinauskas, "Fabrication of micro-tube arrays in photopolymer SZ2080 by using three different methods of a direct laser polymerization technique," J. Micromech. Microeng. **22**(6), 065022 (2012).
24. Y. L. Zhang, Q. D. Chen, H. Xia, and H. B. Sun, "Designable 3D nanofabrication by femtosecond laser direct writing," Nano Today **5**(5), 435–448 (2010).
25. T. C. Chong, M. H. Hong, and L. P. Shi, "Laser precision engineering: from microfabrication to nanoprocessing," Laser Photonics Rev. **4**(1), 123–143 (2010).
26. C. Zhang, Y. Hu, J. Li, G. Li, J. Chu, and W. Huang, "A rapid two-photon fabrication of tube array using an annular Fresnel lens," Opt. Express **22**(4), 3983–3990 (2014).
27. J. A. Davis, E. Carcole, and D. M. Cottrell, "Nondiffracting interference patterns generated with programmable spatial light modulators," Appl. Opt. **35**(4), 599–602 (1996).
28. N. Chattrapiban, E. A. Rogers, D. Cofield, W. T. Hill 3rd, and R. Roy, "Generation of nondiffracting Bessel beams by use of a spatial light modulator," Opt. Lett. **28**(22), 2183–2185 (2003).
29. M. Duocastella and C. B. Arnold, "Bessel and annular beams for materials processing," Laser Photonics Rev. **6**(5), 607–621 (2012).
30. M. Pospiech, M. Emons, B. Väckenstedt, G. Palmer, and U. Morgner, "Single-sweep laser writing of 3D-waveguide devices," Opt. Express **18**(7), 6994–7001 (2010).
31. J. Turunen, A. Vasara, and A. T. Friberg, "Holographic generation of diffraction-free beams," Appl. Opt. **27**(19), 3959–3962 (1988).
32. A. Vasara, J. Turunen, and A. T. Friberg, "Realization of general nondiffracting beams with computer-generated holograms," J. Opt. Soc. Am. A **6**(11), 1748–1754 (1989).
33. C. Paterson and R. Smith, "Higher-order Bessel waves produced by axicon-type computer-generated holograms," Opt. Commun. **124**(1-2), 121–130 (1996).
34. M. V. Berry and K. T. McDonald, "Exact and geometrical optics energy trajectories in twisted beams," J. Opt. A **10**(3), 035005 (2008).
35. C. Xie, R. Giust, V. Jukna, L. Furfaro, M. Jacquot, P. A. Lacourt, L. Froehly, J. Dudley, A. Couairon, and F. Courvoisier, "Light trajectory in Bessel-Gauss vortex beams," J. Opt. Soc. Am. A **32**(7), 1313–1316 (2015).
36. C. Xie, V. Jukna, C. Milián, R. Giust, I. Ouadghiri-Idrissi, T. Itina, J. M. Dudley, A. Couairon, and F. Courvoisier, "Tubular filamentation for laser material processing," Sci. Rep. **5**, 8914 (2015).
37. W. Cheng and P. Polynkin, "Micromachining of borosilicate glass surfaces using femtosecond higher-order Bessel beams," J. Opt. Soc. Am. B **31**(11), C48–C52 (2014).
38. X. Hao, C. F. Kuang, T. T. Wang, and X. Liu, "Effects of polarization on the de-excitation dark focal spot in STED microscopy," J. Opt. **12**(11), 115707 (2010).
39. J. Mačiulaitis, M. Deveikytė, S. Rekštytė, M. Bratchikov, A. Darinskas, A. Šimbelytė, G. Daunoras, A. Laurinavičienė, A. Laurinavičius, R. Gudas, M. Malinauskas, and R. Mačiulaitis, "Preclinical study of SZ2080

material 3D microstructured scaffolds for cartilage tissue engineering made by femtosecond direct laser writing lithography," Biofabrication **7**(1), 015015 (2015).

40. T. Bückmann, N. Stenger, M. Kadic, J. Kaschke, A. Frölich, T. Kennerknecht, C. Eberl, M. Thiel, and M. Wegener, "Tailored 3D mechanical metamaterials made by dip-in direct-laser-writing optical lithography," Adv. Mater. **24**(20), 2710–2714 (2012).

41. K. Obata, A. El-Tamer, L. Koch, U. Hinze, and B. Chichkov, "High-aspect 3D two-photon polymerization structuring with widened objective working range (WOW-2PP)," Light Sci. Appl. **2**(12), e116 (2013).

42. M. Théry, V. Racine, A. Pépin, M. Piel, Y. Chen, J. B. Sibarita, and M. Bornens, "The extracellular matrix guides the orientation of the cell division axis," Nat. Cell Biol. **7**(10), 947–953 (2005).

43. C. Grashoff, B. D. Hoffman, M. D. Brenner, R. Zhou, M. Parsons, M. T. Yang, M. A. McLean, S. G. Sligar, C. S. Chen, T. Ha, and M. A. Schwartz, "Measuring mechanical tension across vinculin reveals regulation of focal adhesion dynamics," Nature **466**(7303), 263–266 (2010).

44. L. Fan, C. Feng, W. Zhao, L. Qian, Y. Wang, and Y. Li, "Directional neurite outgrowth on superaligned carbon nanotube yarn patterned substrate," Nano Lett. **12**(7), 3668–3673 (2012).

45. C. S. Chen, M. Mrksich, S. Huang, G. M. Whitesides, and D. E. Ingber, "Geometric control of cell life and death," Science **276**(5317), 1425–1428 (1997).

46. B. Yuan, Y. Jin, Y. Sun, D. Wang, J. Sun, Z. Wang, W. Zhang, and X. Jiang, "A strategy for depositing different types of cells in three dimensions to mimic tubular structures in tissues," Adv. Mater. **24**(7), 890–896 (2012).

47. M. Jamal, S. S. Kadam, R. Xiao, F. Jivan, T.-M. Onn, R. Fernandes, T. D. Nguyen, and D. H. Gracias, "Bio-origami hydrogel scaffolds composed of photocrosslinked PEG bilayers," Adv. Healthc. Mater. **2**(8), 1142–1150 (2013).

48. S. Chung and K. Vafai, "Effect of the fluid-structure interactions on low-density lipoprotein transport within a multi-layered arterial wall," J. Biomech. **45**(2), 371–381 (2012).

49. S. Bashir, J. Rees, and W. Zimmerman, "Simulations of microfluidic droplet formation using the two-phase level set method," Chem. Eng. Sci. **66**(20), 4733–4741 (2011).

50. O. Thoumine and A. Ott, "Time scale dependent viscoelastic and contractile regimes in fibroblasts probed by microplate manipulation," J. Cell Sci. **110**(Pt 17), 2109–2116 (1997).

51. S. E. Cross, Y.-S. Jin, J. Rao, and J. K. Gimzewski, "Nanomechanical analysis of cells from cancer patients," Nat. Nanotechnol. **2**(12), 780–783 (2007).

52. P. Dalerba, T. Kalisky, D. Sahoo, P. S. Rajendran, M. E. Rothenberg, A. A. Leyrat, S. Sim, J. Okamoto, D. M. Johnston, D. Qian, M. Zabala, J. Bueno, N. F. Neff, J. Wang, A. A. Shelton, B. Visser, S. Hisamori, Y. Shimono, M. van de Wetering, H. Clevers, M. F. Clarke, and S. R. Quake, "Single-cell dissection of transcriptional heterogeneity in human colon tumors," Nat. Biotechnol. **29**(12), 1120–1127 (2011).

53. N. A. Bhowmick, E. G. Neilson, and H. L. Moses, "Stromal fibroblasts in cancer initiation and progression," Nature **432**(7015), 332–337 (2004).

54. R. M. Neve, K. Chin, J. Fridlyand, J. Yeh, F. L. Baehner, T. Fevr, L. Clark, N. Bayani, J. P. Coppe, F. Tong, T. Speed, P. T. Spellman, S. DeVries, A. Lapuk, N. J. Wang, W. L. Kuo, J. L. Stilwell, D. Pinkel, D. G. Albertson, F. M. Waldman, F. McCormick, R. B. Dickson, M. D. Johnson, M. Lippman, S. Ethier, A. Gazdar, and J. W. Gray, "A collection of breast cancer cell lines for the study of functionally distinct cancer subtypes," Cancer Cell **10**(6), 515–527 (2006).

55. E. Charafe-Jauffret, C. Ginestier, F. Iovino, J. Wicinski, N. Cervera, P. Finetti, M. H. Hur, M. E. Diebel, F. Monville, J. Dutcher, M. Brown, P. Viens, L. Xerri, F. Bertucci, G. Stassi, G. Dontu, D. Birnbaum, and M. S. Wicha, "Breast cancer cell lines contain functional cancer stem cells with metastatic capacity and a distinct molecular signature," Cancer Res. **69**(4), 1302–1313 (2009).

56. D. Wu, S. Z. Wu, J. Xu, L. G. Niu, K. Midorikawa, and K. Sugioka, "Hybrid femtosecond laser microfabrication to achieve true 3D glass/polymer composite biochips with multiscale features and high performance: the concept of ship-in-a-bottle biochip," Laser Photonics Rev. **8**(3), 458–467 (2014).

57. D. Wu, J. Xu, S. Z. Wu, L. G. Niu, K. Midorikawa, and K. Sugioka, "In-channel integration of designable microoptical devices using flat scaffold-supported femtosecond-laser microfabrication for coupling-free optofluidic cell counting," Light Sci. Appl. **4**(1), e228 (2015).

58. D. Wu, L. G. Niu, S. Z. Wu, J. Xu, K. Midorikawa, and K. Sugioka, "Ship-in-a-bottle femtosecond laser integration of optofluidic microlens arrays with center-pass units enabling coupling-free parallel cell counting with a 100% success rate," Lab Chip **15**(6), 1515–1523 (2015).

1. Introduction

Microtubes are widely used in the fields of microoptics [1–3], biomedical devices [4–7], microfluidics [8], micropumps [9–11], microsensors [12–14] and cell biology [12, 15]. In the field of microoptics, microtubes fabricated from glass capillary tubes are used for focusing light in the subwavelength level. Fu et al. [2] reported a focal spot of size ~435 nm at a distance of ~1.47 μm from the output end. Microtubes in the optical mode have been used as optical ring resonators [3]. In the field of biomedical devices, microtubes are widely used as microneedles for drug delivery. The relationship between the geometry of the microtube and the liquid flow properties is investigated in [5, 6]. In microfluidics, microtubes are integrated

into a microfluidic device by photolithography for integrative fluid analysis on a chip [8]. Microtubes can also be used as self-propelling micropumps in cargo transportation, which is a promising way to construct versatile and intelligent tubular microrobots [9]. In microsensor development, microtubes are enclosed and patterned with a SU-8 polymeric matrix to form an integrated tubular optofluidic sensor, which has high sensitivity to refractive index changes [13]. Impedimetric microsensors are developed by integrating Au-base electrodes on microtubes for determining the in-flow of monovalent and divalent ionic species and HeLa cells [14]. Two-dimensional cultures such as patterned planar substrates are often used for cell biology study. However, cellular processes usually happen in 3D spatially confined physiological environments. Microtubes are used to encapsulate single cells to provide a confined 3D microenvironment for the analysis of cellular dynamics, which determines the proliferation, growth, apoptosis, and differentiation of a cell [9, 12].

Several methods have been developed for the fabrication of microtubes. Schmidt fabricated microtube arrays by using the self-rolling property of organic and inorganic films [16–18]. However, only straight microtubes can be fabricated due to the intrinsic character of the technology. Microtubes can also be manufactured by the continuous accumulation of nanoparticles; this is achieved by guiding the meniscus upward in a solution of nanoparticles [19]. However, this technology results in microtubes that exhibit poor uniformity and weak strength. Electrospinning is a straightforward and cost-effective method to produce microtubes. However, using this method, only one-dimensional microtubes can be produced and it is difficult to control their size [20]. Other methods include mask-based diffraction lithography [21], template base deposition [22], and holographic lithography [23]. However, these methods also lack flexibility. Femtosecond two-photon polymerization (TPP) is a promising tool for the fabrication of microstructures of arbitrary size [24–26]. In this method, the microstructures are prototyped by point-to-point scanning. Nevertheless, this technique too has a serious drawback in that the processing time scale increases as the third power of the object size, which is unacceptable for the fabrication of large-area microtube arrays.

In this paper, we present a fast and flexible approach for the fabrication of large-area microtube arrays and demonstrate its use in single cell study. This objective is realized in three steps. First, a femtosecond laser beam is modulated into several Bessel beams by a liquid crystal spatial light modulator (SLM) and then focused into resin for TPP. Then, microtubes are effectively fabricated by scanning the focused Bessel beam along a designed route. The dimension and geometry of microtubes are controlled by tuning the fabrication parameters. This technology retains the high resolution of the TPP approach while reducing the processing time by two magnitudes. Finally, the fabricated microtube is used for the capture and release of particles and cells. This demonstrates that the proposed method is a promising way to study single cell biology in a confined 3D microenvironment that closely resembles the in vivo conditions.

2. Experimental procedure

2.1 Generation and focusing of femtosecond laser Bessel beam using hologram imprinted SLM

The Bessel beams are generated using a SLM with loaded holograms that have a transmission function

$$T_n(r, \theta) = \exp(in\theta)\exp(-i2\pi r / r_0), \tag{1}$$

where r and θ are the transverse and polar coordinates respectively, n is the n-th order Bessel beam, and r_0 is an adjustable constant parameter [27–29]. Equation (1) can be divided into two terms. The first term is associated with the azimuthal phase. The second term generates the zeroth order Bessel beam. Since the SLM display comprises of pixels, we

rewrite r as $r = (i^2 + j^2)^{1/2}\Delta$, where i and j are integers that indicate each SLM pixel, and Δ is the pixel pitch. In the experiment, a blazed grating pattern with phase $\phi_{grating}$ is directly added with the hologram for Bessel beam generation to separate the Bessel beam from zero diffraction order. The phase $\phi_{grating}$ required to produce a lateral shift is calculated by

$$\phi_{grating}(i,j) = 2\pi(\frac{i}{\Gamma} + \frac{j}{\Gamma}),$$ (2)

where Γ is the period of blazed grating [30]. The final phase pattern loaded to the SLM is:

$$\phi_{holo} = (T_n + \phi_{grating}).$$ (3)

According to the grating theory, the diffraction angle of the 1st order, γ, can be derived as $\sin\gamma = \lambda/\Gamma$, where λ is the wavelength of incidence and is. In our study, the Bessel beam is 8 mm shifted from the zero order at a distance of 1.2 m from the SLM. The incidence in our experiments is assumed to be Gaussian beam with plane wave front. The electric field at a distance z behind SLM is derived from Fresnel diffraction theory:

$$E(\rho,\varphi,z) = -\frac{\exp(ikz)}{ikz}\exp(\frac{ik\rho^2}{2z})\int_0^R\int_0^{2\pi}T_n(r,\theta)\exp(\frac{ikr^2}{2z})\exp[\frac{-ikr\rho\cos(\theta-\varphi)}{z}]2\pi rdrd\theta.$$

(4)

Here ρ and φ are polar coordinates in the observation plane, and R is the radius of the hologram. Substituting Eq. (1) into Eq. (2), performing the angular integral, and using the integral definition of Bessel functions, the electric field is derived as:

$$E(\rho,\varphi,z) = \frac{\lambda^{2.5}}{i^{2.5}r_0}z^{1/2}J_n(\frac{2\pi\rho}{r_0})\exp\{i[kz + n(\phi - \frac{\pi}{2}) + \frac{\pi\lambda z}{r_0^2} + \frac{k\rho^2}{2z}]\}.$$ (5)

where J_n is the n-th order Bessel function of the first kind [27,31–37]. The intensity profile of the generated beam is proportional to the square of the Bessel function. The most remarkable advantage of this SLM-based approach is that the parameters of the Bessel beam can be flexibly controlled by adjusting n and r_0.

   Then, Bessel beam is focused with a high numerical aperture (NA) objective. Since the paraxial approximation does not consider the vectorial nature, the optical field at the focusing region is calculated by Debye vectorial diffraction theory, which describes the depolarization effect of a high-NA objective by calculating the three orthogonal field components Ex, Ey and Ez, respectively [38] and is derived as:

$$E_2(x_2,y_2,z_2) = -\frac{iC}{\lambda}\int_0^\alpha\int_0^{2\pi}\sin\theta_2 E(\theta_2,\varphi_2,z_{obj})\sqrt{\cos\theta_2}\mathbf{P}(\theta_2,\varphi_2)$$
$$\exp[ikn_{diff}(z_2\cos\theta_2 + x_2\sin\theta_2\cos\varphi_2 + y_2\sin\theta_2\sin\varphi_2)]d\theta_2 d\varphi_2.$$

(6)

Here C is a constant, $k = 2\pi/\lambda$ is the wave number; λ is 800 nm, the wavelength of incident light; n_{diff} is 1.518, the refractive index of immersion medium; α is the maximum focusing angle of the objective lens and can be calculated according to formula: $\alpha = \arcsin(NA/n_{diff})$. NA is the numerical aperture of objective lens, θ_2 represents the focusing angle of objective lens and φ_2 is the azimuthal angle of object plane. z_{obj} is the

distance between objective and SLM, which is 1.6 m in this work. $\mathbf{P}(\theta_2, \varphi_2)$ indicates the polarization state of the EM field in the focal region, which can be rewritten as:

$$\boldsymbol{P}(\theta_2, \varphi_2) = [1 + (\cos\theta_2 - 1)\cos^2\varphi_2]\mathbf{i} + [(\cos\theta_2 - 1)\cos\varphi_2\sin\varphi_2]\mathbf{j} - \sin\theta_2\cos\varphi_2\boldsymbol{k} \quad (7)$$

for incidence with linear polarization at X direction, as used in our experiment. The field described by Eq. (6) and Eq. (7) is represented in Fig. 1(b).

2.2 Fabrication of large-area 3D microtube arrays using scanning of focused femtosecond laser Bessel beam

In this study, the laser source used in the fabrication system is a femtosecond laser with a central wavelength of 780 nm (Chameleon Ultra, Coherent Corp., repetition rate: 80 MHz, pulse width < 140 fs). The laser power is controlled using a half-wave plate combined with a polarization beam splitter. After passing through a beam expander, the laser beam illuminates a reflection type liquid crystal SLM (Pluto NIRII, Holoeye, 1920 × 1080 pixels, 256 grey levels, pixel pitch of 8 μm), on which the calculated holograms are encoded. Due to the Gaussian distribution of the incident laser, the femtosecond laser beam expands and becomes larger than the SLM display; only the central 1080 × 1080 pixels are used for phase modulation. The femtosecond Bessel beam is generated using the SLM and the zero order is filtered before being focused onto a sample with a high numerical aperture objective (60 × , NA = 1.35, Olympus) for TPP polymerization. The sample is prepared by drop casting SZ2080 photoresist onto a cover glass and then baking on a hot plate for 1 hour. SZ2080 is chosen here because of its biocompatibility [39]. The sample is anchored to a 3D stage (E545, Physik Instrument), which is controlled along with a shutter (SC10, Thorlab) using a computer. The fabrication process is monitored in situ with a charge coupled device (CCD) camera. After the microtubes are fabricated, the sample is developed in normal propyl alcohol for half an hour and then dried by natural evaporation in air. To avoid the collapse of microtubes due to perturbation of liquid developer and surface tension, the sample is placed upside down when developing and drying. The samples are sputter coated with Au for 120 s and imaged with an Environment Scanning Electronic Microscope (ESEM, XL-30, FEI, America).
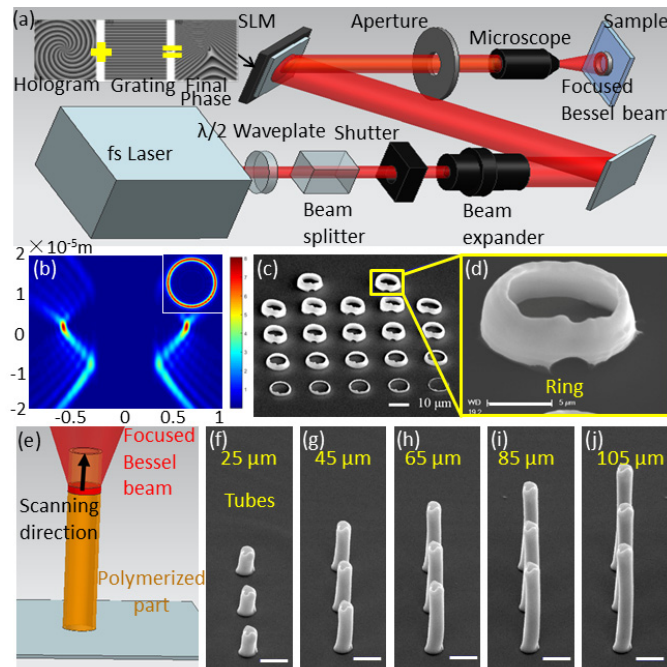
Fig. 1. High efficiency fabrication of microtubes by focused femtosecond laser Bessel beam scanning. (a) Femtosecond Bessel beam is generated by phase modulation using a predesigned hologram loaded in the SLM. The inset shows the combination of blazed grating and hologram for a Bessel beam to separate the Bessel beam from the zero diffraction order. (b) The intensity distribution at the focal region of a focused 20th order Bessel beam. The inset shows the intensity distribution at the focal plane. (c) Cylindrical microstructures fabricated by ascending the focal plane line-by-line. In the fifth line, only two cylinders are left and this is the critical position where the cylinder adheres to the substrate. (d) Magnified SEM images of polymerized cylindrical microstructure generated in a single shot. The scale bar is 5 μm. (e) Schematic of the new strategy for rapid fabrication of microtube by scanning focused Bessel beam. (f)-(j) Microtubes fabricated with height of 25 μm, 45 μm, 65 μm, 85 μm, and 105 μm, respectively. Focused 20th order Bessel beam is used for single exposure of cylindrical microstructure in (c)-(d) and for the fabrication of microtubes in (f)-(j). The scale bars are 20 μm.

Figure 1(a) shows the modulation of the femtosecond laser beam into several Bessel beams by loading holograms into the SLM. Any Bessel beam between the 20th and 40th order can be used to fabricate cylindrical microstructures as the beams in this range provide suitable intensity profiles for TPP production. By focusing femtosecond Bessel beams using a high numerical aperture, a cylinder optical pattern is generated at the focal plane [Fig. 1(b)]. This is used for producing cylinder microstructures in photoresist materials [Figs. 1(c) and 1(d)]. In this work, we propose a new approach for fabricating microtubes based on the designed Bessel beams. By simply moving the sample along the direction of light propagation, microtubes can be rapidly fabricated [Fig. 1(e)]. In contrast to the conventional point-to-point process that fabricates microtubes in a layer-by-layer fashion using overlapping single voxels, microtubes are manufactured by the rapid scanning of a cylindrical laser pattern in our method.

Since the fabrication time is significantly reduced using this technique, microtubes with large-area (1 mm^2) can be realized. We analyze the size of a polymerized cylindrical structure generated by a single shot [Fig. 1(c)]. This is performed by using the ascending scan technology, which has been widely used by researchers for investigating the size of a single voxel in the TPP process. Cylindrical microstructures are polymerized while the focal plane ascends from the bottom to the top of the substrate surface. The power and exposure time are

all the same. The only difference between different lines is the position of focal plane. For the first line, only a small part of focal pattern is above the substrate. The focal pattern ascends for the following lines, and is fully above the substrate for the last line. When the focal pattern continue to ascend, the polymerized structure by single exposure will not attach to the substrate and finally been flushed away in the development procedure. Using this method, we obtain complete cylindrical microstructures that adhere to the substrate, preventing them from getting flushing away during development. This is shown in Figs. 1(c) and 1(d). The height and diameter of a cylinder microstructure polymerized using a Bessel beam with laser power of 50 mW and an exposure time of 500 ms is measured to be 6 μm and 11.8 μm. The microtubes from Fig. 1(f) to Fig. 1(j) were fabricated with different scanning duration, while the other fabrication parameters including laser power and scanning speed were kept constant. When the scanning speed is fixed to be 40 μm/s, the height of microtubes from 25 μm to 105μm can be precisely controlled by quantitatively setting the scanning duration from 625 ms to 2625 ms.. 20th order Bessel with laser power of 100 mW and a scanning speed of 40 μm/s is used for the microtube fabrication. The laser is sent through the substrate and microtube growth is performed on the exit side. The height limitation of microtube is decided by the work distance of objective used in the experiment system because the deepest distance that the laser beam can focus in the photoresist is the work distance of objective lens. In our system, we used a 60 × U plan super apochromat objective (Olympus) with a work distance of 0.15 mm, which means the ultimate range of microtube height is 0-150 μm. This height limit can be overcome by Dip-in laser writing technique [40] or WOW-2PP technique [41] if liquid photoresist is used.
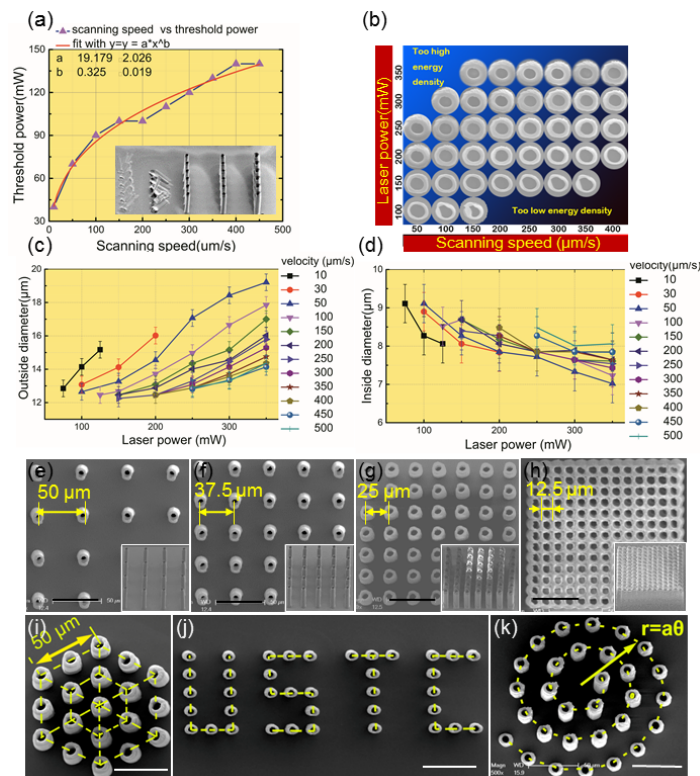

Fig. 2. Controlled fabrication of microtube arrays by quantitatively tuning the fabrication parameters (a) The threshold power P at different scanning speeds v. (b) The variation of external physical characteristic of the microtubes with different fabrication parameters. (c)-(d) The relationship between tube diameters and laser power for different scanning speeds.

2.3 Quantitative investigation of focused Bessel beam scanning parameters for controllable microtube arrays

Systematic investigation of the experimental parameters is necessary for fabricating high quality microtubes using the femtosecond laser Bessel beam. For a specific scanning speed, we find that there is a threshold laser power, below which TPP cannot occur or microtubes do not have enough strength to survive after developing. The threshold power P for different scanning speeds v is shown in Fig. 2(a) and the approximate fitting between P and v is $P = 19.17849 \times v^{0.32491}$.

The outer and inner diameters of the microtubes fabricated using a specific focused Bessel beam are related to fabrication parameters such as the laser power and scanning speed. We performed a series of experiments to analyze the variation of external physical tube characteristics with respect to the fabrication parameters. The results are shown in Fig. 2(b). Additionally, the relationship between the diameter of the tubes and the laser power for different scanning speeds is studied [Figs. 2(c) and 2(d)]. We increased the laser power from 50 mW to 350 mW in increments of 50 mW, and the scanning speed from 10 μm/s to 500 μm/s. It was observed that the outer diameter increases and the inner diameter decreases with increase in the laser power and decrease in the scanning speed. We could vary the outer diameter in the range of 12-20 μm and the inner diameter in the range of 6-10 μm. In Fig. 2, all the microtubes have a height of 100 μm, which are fabricated with a scanning speed of 40 μm/s and illumination time of 2.5 s. Moreover, we were also able to control the periods and distribution of microtubes in the array. As shown in Figs. 3(a)-3(d), microtubes with various periods of 50 μm, 37.5 μm, 25 μm, and 12.5 μm were fabricated. Figures 3(e)-3(j) show microtubes in various patterns, specifically as a hexagon with 25 μm space, a "USTC" pattern, and an "Archimedes spiral." The "Archimedes spiral" microtube array was designed by varying the microtube heights from 5 μm to 150 μm; it is very challenging to generate this using other techniques. This shows the distinct advantages of our approach in terms of flexibility, and 3D and customization capabilities.
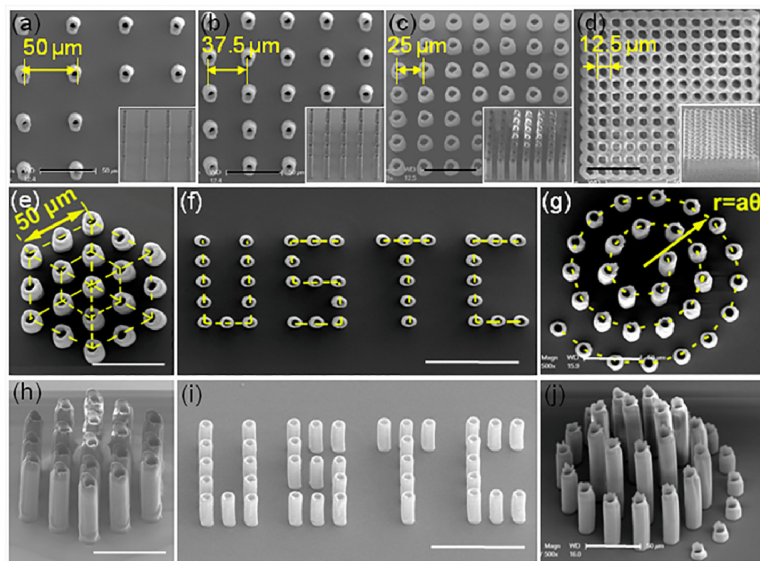

Fig. 3. Customized fabrication of microtube arrays by quantitatively tuning the fabrication parameters (a)-(d) Microtubes with periods of 50 μm, 37.5 μm, 25 μm, and 12.5 μm, respectively. The height of microtubes is 75 μm. (e)-(h) Microtubes with hexagonal distribution and 25 μm space (f)-(i) Microtubes arranged in an "USTC" pattern (g)-(j) Microtubes in a 3D "Archimedes spiral" with height increasing linearly. The scale bars are 100 μm in cases (f) and (i), and 50 μm in the other figures.

2.4 Tilted scanning of focused femtosecond laser Bessel beam to generate complex flower-like microtube arrays

The blood vessels and other tubular systems in the body have complex geometries and are usually not straight tubes. Hence, in addition to straight microtubes that are perpendicular to the substrate, we also fabricated slant microtubes by directing the scanning focused Bessel beam along a 3D route. Figures 4(a)-4(c) show the schematic diagrams of the focused light field scanning in different directions and the fabricated microtubes with slant angles of 15°, 30°, 45°, and 60°, respectively. By changing the scanning speeds along three directions in real time, the focused Bessel beam can be made to scan in a more complex route and thus 3D microtubes with zigzag profile were fabricated [Fig. 4(c)]. The tilt angle is controlled by the ratio of speeds in the X, Y, and Z directions. Moreover, by positioning microtubes with different slant directions and angles, flower-like microtube clusters with 4, 7, and 13 petals were fabricated, as shown in Figs. 4(d)-4(i). We can find that the surfaces roughness increase for the tilted microtubes. This is because that the accumulation of laser exposure are different at different side of microtube when scanning focused Bessel beam along a tilt angle, as there is a divergence angle of focused Bessel beam.
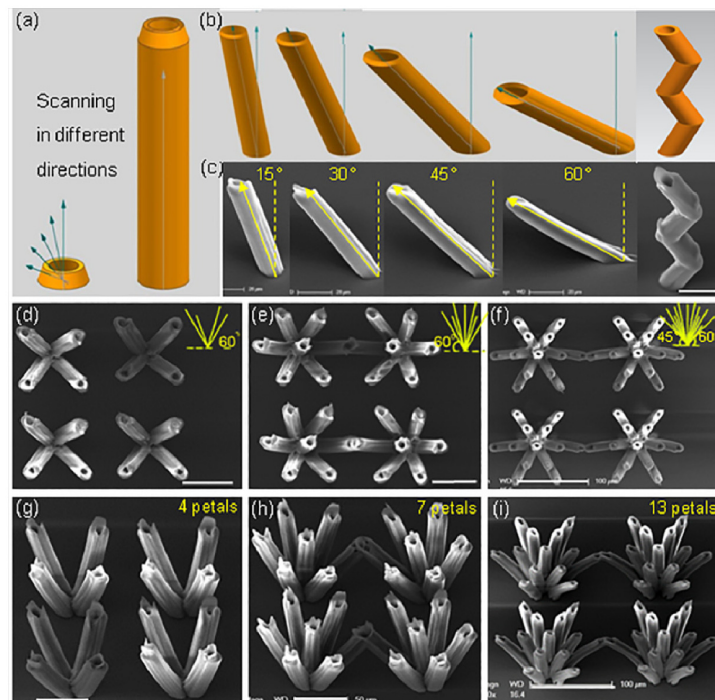

Fig. 4. 3D slant microtubes and flower-like microtube arrays fabricated by tilted the Bessel beam scanning. (a)-(b) Schematic diagrams of the focus light field scanning in different directions. (c) Fabricated microtubes with slant angles of 15°, 30°, 45°, and 60°, and the zigzag microtube. (d)-(f) Flower-like microtube cluster with 4, 7, and 13 petals respectively. (g)-(i) Tilted view of (d)-(f).The scale bars are 20μm in (c), 50 μm in (d), (e), (g), and (h), and 100 μm in (f) and (i).

2.5 Capturing microparticles and NIH3T3 cells using microtube arrays

Effective control and study of single cell behaviors in spatially confined environments is of great importance in cell biology, material-cell interactions, and bio-physics [42–45]. Microtubes can be used for the capture and release of cells for single cell research [9, 46, 47]. In our study, we designed and fabricated closely packed microtube arrays to increase the possibility of cell capture and convenience of micro-manipulation. Figure 5(a) depicts our in-

house micro-manipulation system used for cell capture, which consists of a microneedle, an XYZ micro-manipulator, and a syringe. By aspirating using a syringe, it is possible to capture cells efficiently using the microtubes [The inset of Fig. 5(a)]. Cover glass, the medium on which microtubes are fabricated, is stuck to the bottom of a petri dish. Culture media containing cells are dropped around the microtubes. The petri dish is placed on a fluorescence inversion microscope (DMI3000B inverted microscopy, Leica). The whole capture and release process is monitored using a CCD camera. A micropump, depicted in Fig. 5(a), is used to capture and release cells suspended within the culture. The micropump consists of a microneedle (inner diameter 60 μm, outer diameter 190 μm), an XYZ micro-manipulator, and a syringe. The microneedle is fixed to the XYZ micro-manipulator and connected to the syringe with a plastic hose; its tip is positioned at one end of the microtubes. After the microneedle is in place, the syringe is used to perform aspiration.

To implement cell capture and release, microtubes need to be pushed down to form through microtubes. There are two effective ways to push down the microtubes. The first way is to let the microtubes fall down by themselves under the influence of surface tension and perturbation of the liquid developer. In this method, it is critical to control the starting point of TPP fabrication. The point should be close enough to the basement to ensure that the microtubes are connected to the basement, while making sure that the connection is not too tight. However, in this method, it is hard to control the starting point, the microtubes may be flushed away while developing, or they might keep standing. In the second technique, microtubes are pushed down using a microneedle fixed to the XYZ micro-manipulator in the cell capture system. Although the microtubes that are pushed down using external forces may not adhere to the substrate tightly, this method allows us to control the parameters and is hence preferable. Linear microtube arrays [Fig. 5(b)] are fabricated to improve adhesion to the substrate and used for the subsequent particle/cell manipulation.
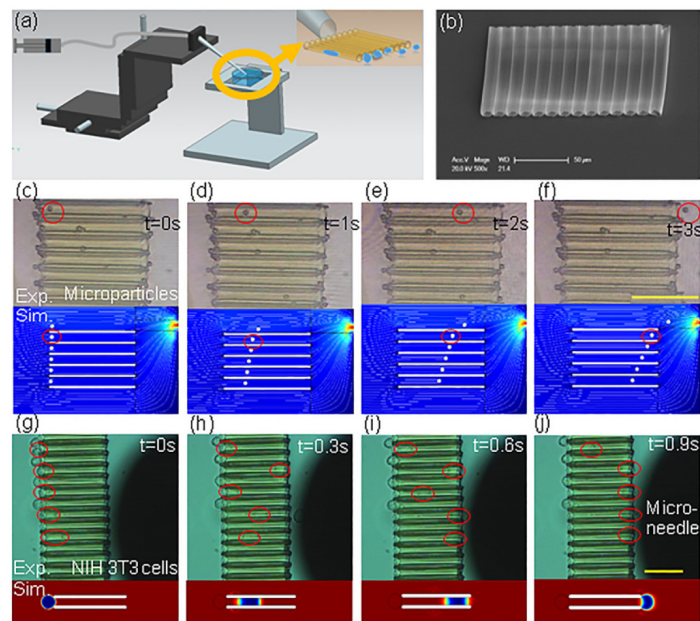

Fig. 5. Capture of SiO₂ microparticles and NIH 3T3 cells. (a) Schematic diagram of the micropump system for the capture and release of microparticles and cells. (b) SEM of close-packed microtube array. (c)-(f) Experimental process and the simulated progress of SiO₂ nanoparticles being captured by the microtube and passing through slowly by pumping with syringe. Microtubes on a chip are placed in a culture medium rich of SiO₂ microparticles. The scale bar is 50 μm. (g)-(j) NIH 3T3 cells are captured into microtubes for single cell research. The scale bar is 50 μm.

The microtubes are first used for trapping SiO_2 microparticles of diameter 3.8 μm in deionized water. As shown in the experimental [Figs. 5(c)-5(f)] and simulation results generated using a commercial software COMSOL (see Visualization 1), microparticles move with a fixed velocity that increases with proximity to the microneedle. In this study, we use NIH 3T3 fibroblast mouse cells for single cell study, as they are highly sensitive to mechanical changes. NIH/3T3 mouse fibroblasts were cultured in DMEM supplemented with 1% streptomycin/penicillin and 10% fetal bovine serum (all from Gibco, USA), and incubated in an environment of 5% CO_2, 37 °C in 60 mm dishes. They were then treated with Trypsin-EDTA (Gibco, USA) solution after they became confluent for 1 minute. In the cell capture experiment, microtubes are placed in a medium rich in NIH 3T3 cells. A syringe is used to aspirate at one end, causing the cells to align at the other end of the microtube. They are then slowly sucked into it [Figs. 5(g)-5(j)]. Once the cells are completely sucked in, aspiration is stopped and the cells are thus captured. Cells that are larger than the inner diameter of the microtubes (see Visualization 2) are sucked in in a deformed manner. At the end of the aspiration, the NIH 3T3 cells are successfully captured and stay in the microtubes. This allows researchers to study single cell behaviors in a confined environment. To release the cells, the sample is taken out from the culture and put into another petri dish filled with culture. The tip of the microneedle is positioned at the end from which cells are sucked in. By aspirating with the syringe, the cells are slowly released from the microtubes.

The relationship between the migration distance and the duration in the progress of SiO_2 microparticles and NIH 3T3 cells in the microtubes is shown in Figs. 6(a) and 6(b). Microparticles in a specific tube exhibit almost uniform motion with a fixed velocity. Due to the neglection of friction between microparticles and the tube's bottom, there are small differences between the simulated velocity and the experimentally measured velocity. NIH 3T3 cells move in a completely different way, which can be divided into three phases. In the first phases, NIH 3T3 cells that are just sucked into the microtubes move slowly. In the second phase, the NIH 3T3 cells move rapidly and cover a long distance in a short time. Finally, when the NIH 3T3 cell is close to the exit of microtube the velocity decreases dramatically. The diameters of microtubes are smaller than those of cells. Hence, cells are deformed before they are sucked into and pumped out from the tubes, which comes out that the cells enter and exit slowly.This is consistent with the simulation results. (see Visualization 3).
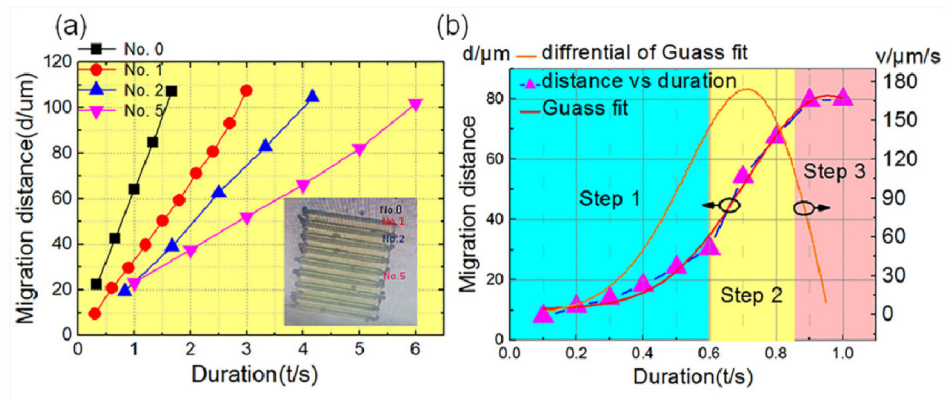

Fig. 6. Movement of SiO_2 microparticles and NIH 3T3 cells in the microtubes (a)-(b) Relationship between migration distance and time duration in the progress of SiO_2 microparticles and NIH 3T3 cells in the microtubes.

2.6 Simulation of the movement of microparticles and NIH3T3 cells in microtube arrays

By modeling the process of capturing microparticles and cells in COMSOL, some characteristics of the capture process can be verified. The capture progress of microparticles and cells is simulated using COMSOL, a commercial software. In the simulation of capturing the microparticles, the motion of solid microparticles in a fluid was modeled and the fluid-structure interaction model [48] is adapted. Microparticles were considered as SiO2 with the similar physical property. The fluid flow in the channel was described by the incompressible Navier-Storkes equations. Slip boundary condition and constant pressure are assumed. The fluid speed in the microtubes is found to be related to the distance between the microtubes and the aspirating needle. As the diameter of SiO_2 microparticles is smaller than the inner diameter of microtubes, the speed ratio of microparticles is coincident with the flow velocity ratio between different microtubes.

In contrast to this, the diameter of the NIH 3T3 cells is in the range of 8~12 μm, while the inner diameter of microtubes is 8 μm. We neglect the extrusion deformation of the nucleus. In the simulation of cell capture, the motion of fluid was modeled and two-phase laminar flow model [49] were used. Cells are treated as liposome, having a flow phase with a high viscosity of 2000 Pa*s [50]. We gave a high surface tension to prevent the cell phase diffusion or fission. Level set interface automatically set up the equations for the convection of the interface. The density of cells is set to be a little greater than that of water. Assuming that cells maintain a spherical shape in the free state, a surface tension at the interface of the cell and surrounding phase is applied to simulate the constriction of the cell membrane. Slip boundary condition is used for all the microtube shells.

2.7 Multifunctional micromanipulation (capture/transfer/release) of cancer cells using microtube arrays

Study of the motility, growth, and proliferation of cancer cells in a confined environment close to that of the body in vivo environment is of significant importance for cancer research [51–53]. SUM159 triple-negative breast cancer cells were extensively characterized in [54]. In our study, cell lines were grown in 60 mm petri dishes (Thermo Fisher Scientific, USA) using the recommended culture conditions as described in [55]. Then, the cells lines were treated with Trypsin-EDTA (Gibco, USA) solution after they became confluent for 1 minute. Cell suspensions were then centrifuged at a rate of 1000 rounds per minute for 5 min in a centrifuge tube. New culture media were added after removing the supernatant. The cells were resuspended by gently pipetting 5 times. Coverslips with the fabricated structures were placed in 35 mm petri dishes and immersed in 2 mL of the former cell suspension.

Using the procedure described previously, we conducted a series of experiments on the capture, transfer, and release of breast cancer cells [Fig. 7]. First, the cancer cells were captured using the procedure followed for NIH 3T3 cell capture; this is marked with a yellow circle in Fig. 7(f). Then, the microtubes together with substrate were transferred to another medium [Figs. 7(g)-7(i)]. From observing the transferred cells using an optical and fluorescence microscope [Figs. 7(h) and 7(i)], we found that cells outside the microtubes were diluted, while the captured cells were stable inside the microtubes. To release the captured cancer cells, the tip of the microneedle was positioned at one end of the microtube. Using a syringe, the cancer cells were aspirated slowly and released into the medium [Figs. 7(j)-7(l) and see Visualization 4].
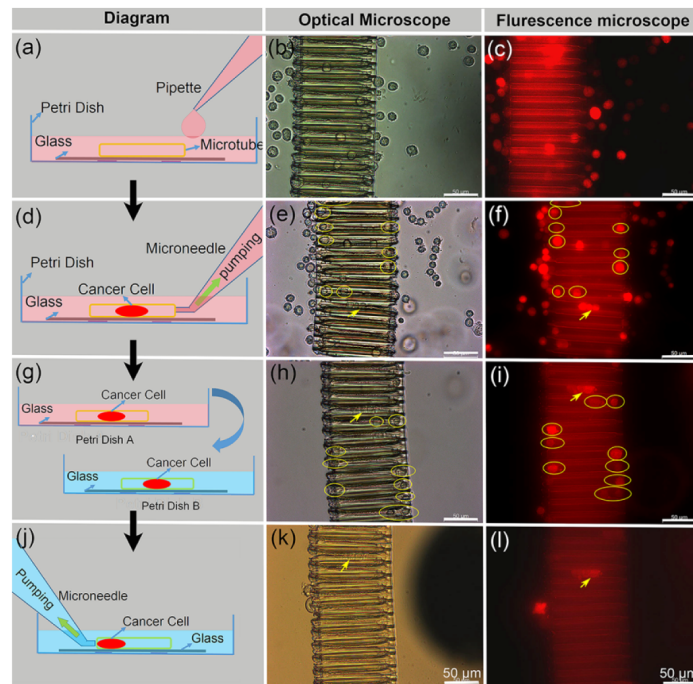
Fig. 7. Capture, transfer, and release of breast cancer cells. (a) Immersion of microtubes into a medium containing breast cancer cells (b)-(c) Optical and fluorescence microscope images of microtubes immersed into cancer cell medium (d) Capture of breast cancer cells into microtubes using the micro-manipulation system (e)-(f) Optical and fluorescence microscope images of breast cancer cells captured in microtubes. The captured cancer cells are marked with a yellow circle. The yellow arrow points to a group of three captured cells, which serves as a position mark. (g) Transfer of microtubes along with the cover glass to another environment. (h)-(i) Preservation of the captured cancer cells in microtubes after the transfer operation. (j) Cell release process (k)-(l) Microtube after releasing the cancer cells

3. Conclusion

In this paper, we proposed a novel approach for rapid and flexible fabrication of complex 3D microtubes using a focused femtosecond Bessel beam. A liquid crystal SLM was used to convert a femtosecond laser beam into Bessel beams for the two-photon polymerization of microtubes. The dimension, geometry, and distribution of microtubes were precisely controlled by varying the parameters of the fabrication process. The fabrication efficiency was enhanced by two orders of magnitude in comparison with the conventional point-to-point scanning. The ability of the fabricated microtubes to participate in the accurate trapping, transfer, and release of microparticles as well as cells was demonstrated. The proposed focused Bessel beam scanning technique and the fabricated microtubes provide the first step toward the creation of customized spatial platform mimicking complex 3D biological environments, which creates new opportunities for lab-on-a-chip systems [56–58] and in vitro study of single cell behaviors.

Funding